Forces generated during actin-based propulsion: A direct measurement by micromanipulation

Yann Marcy[†], Jacques Prost[†], Marie-France Carlier[‡], and Cécile Sykes[†§]

[†]Laboratoire Physico-Chimie Curie, Unité Mixte de Recherche 168 Institut Curie, Centre National de la Recherche Scientifique, 11 Rue Pierre et Marie Curie, 75231 Paris Cedex 5, France; and [‡]Dynamique du cytosquelette, Laboratoire d'Enzymologie et de Biologie Structurale, Centre National de la Recherche Scientifique, 91198 Gif-sur-Yvette, France

Edited by Edward D. Korn, National Institutes of Health, Bethesda, MD, and approved March 3, 2004 (received for review November 20, 2003)

Dynamic actin networks generate forces for numerous types of movements such as lamellipodia protrusion or the motion of endocytic vesicles. The actin-based propulsive movement of *Listeria monocytogenes* or of functionalized microspheres have been extensively used as model systems to identify the biochemical components that are necessary for actin-based motility. However, quantitative force measurements are required to elucidate the mechanism of force generation, which is still under debate. To directly probe the forces generated in the process of actin-based propulsion, we developed a micromanipulation experiment. A comet growing from a coated polystyrene bead is held by a micropipette while the bead is attached to a force probe, by using a specially designed "flexible handle." This system allows us to apply both pulling and pushing external forces up to a few nanonewtons. By pulling the actin tail away from the bead at high speed, we estimate the elastic modulus of the gel and measure the force necessary to detach the tail from the bead. By applying a constant force in the range of −1.7 to 4.3 nN, the force–velocity relation is established. We find that the relation is linear for pulling forces and decays more weakly for pushing forces. This behavior is explained by using a dimensional elastic analysis.

The growth of a polymer against a barrier is a general mechanism for production of force in cell biology (1). Spatially controlled polymerization of actin is responsible for a large variety of changes in cell shape leading to cell movement, like the protrusion of the lamellipodium (2), or the intracellular propulsion of vesicles (3, 4) and pathogens (5, 6). Actin assembly in these processes is controlled by various proteins present in the cytoplasm, which have been identified over the last 10 years (see refs. 7 and 8 for review). It is now well established that the Arp2/3 complex associates with Wiskott–Aldrich Syndrome protein (WASp) family proteins to create new filaments locally by branching them (9), thus generating the dendritic organization of the actin array (10, 11). Because pure actin treadmilling is too slow to account for polymerization speed observed in these systems, this process has to be speeded up by regulatory proteins (8). One experimental model that has been used widely for the identification of these proteins is the bacteria *Listeria monocytogenes*, which are propelled inside cells by actin polymerization. The minimal subset of proteins necessary and sufficient to reconstitute the *Listeria* movement has been identified (12). In addition to Arp2/3 and actin, the regulatory proteins ADF/cofilin, profilin, and a capping protein are necessary to enhance the efficiency of treadmilling (13) and control the life time and average length of filaments (14, 15). The essential role of these proteins has been confirmed recently (16) *in vivo* by using a RNA interference strategy.

Biomimetic systems are useful for analyzing the physical aspects of actin-based motility. *Listeria* movement can be mimicked by functionalized polystyrene beads catalyzing filament branching at their surface and undergoing actin-based propulsion when placed in cell extracts or in the reconstituted motility medium. These systems have been used to characterize the process of actin comet formation (17), to measure the elastic properties of actin gels growing from a surface (18), and to explore the dynamical regimes of actin-based propulsion by varying the size of the bead (19). In a mixture of purified proteins that reconstitute *Listeria* movement, beads activating actin polymerization move in a wide range of size (up to 10 μm diameter) and display various types of movement (19). This is an advantage over the *Listeria* system in which such parameters cannot be changed. Within a cell, micrometer size objects moving at a velocity of the order of a few micrometers per minute have to oppose the viscous force (Stokes force) of 1 fN. Indirect approaches have been developed recently to evaluate the magnitude of the propulsive force. Increasing the viscosity of the medium by several orders of magnitude only slightly slowed down bead movement (20), suggesting that the propulsive force is much larger than 50 pN. This result is in disagreement with the reported observation of a dramatic decrease in *Listeria* velocity under a 0–50 pN viscous force (21). Other experiments however (22, 23) suggested that the propelling force is much larger, of the order of few nN. Likewise, the force exerted by the lamellipodium on a moving cell is of the order of a few nN (24). The discrepancies described above call for direct measurements of the force generated by actin polymerization, which are carried out here. To exert a relevant range of forces, actin-propelled beads are micromanipulated by using a flexible handle as a force probe and a micropipette to hold the tail. By using this design, various experiments can be performed because either the force or the pulling velocity can be controlled whereas the bead and the comet can be visualized optically during the experiment. We measure the force required to detach the actin tail from the bead and estimate the comet elastic modulus. Furthermore, we produce a force–velocity diagram in the range of pulling (−1.7 nN) to pushing (4.3 nN) forces. This experimental setup allows for a direct, *in situ* measurement of the force generated in actin-based propulsion.

Materials and Methods

Micropipettes. Micropipettes (Fisher Scientific) were prepared with a P2000 pipette puller (Sutter Instruments, Novato, CA). Their tip was broken by insertion in a molten drop of soda-lime glass (25) by using a microforge (Narishige, Tokyo) with a ×60 objective (Olympus, Melville, NY) to allow inner-tip diameter control. Micropipettes designed for bead holding had an inner diameter of ≈1.5 μm. Micropipettes that were used to functionalize beads were 4.5 μm in diameter. The tip of micropipettes used to hold the actin tail was narrowed, by an additional heating step, to an internal diameter of 1.5 μm, with a surrounding 3.5-μm discoid wall.

Glass Fibers. Two different fibers were obtained from either glass rods or glass wool microfibers. Glass rods (1-mm diameter;

This paper was submitted directly (Track II) to the PNAS office.

Abbreviations: PDMS, poly(dimethyl siloxane); WASp, Wiskott–Aldrich Syndrome protein.

§To whom correspondence should be addressed. E-mail: cecile.sykes@curie.fr.

World Precision Instruments, Sarasota, FL) were pulled to a taper length of 1.5 cm. The tip of the rod was broken at a 1.5-μm diameter by using the same process as for micropipettes. The tapered rods were etched in HF (10% in water) for 9–12 min to reduce the end diameter to tens of micrometers in a reproducible way (26). Microfibers from glass wool (Lauscha Fiber, Lauscha, Germany) were dispersed in water and dried on a microscope slide. One microfiber (100–500 μm long, ≈0.3-μm diameter) was caught with a glass microneedle and inserted into the tip of a micropipette (3-μm inner-tip diameter) filled with optical glue. The microfiber was then immobilized by polymerizing the glue.

Optical Bonding. NOA68 optical glue (Norland Products, Cranbury, NJ) was used to hold microfibers in micropipettes, to attach the beads to the fibers, and to fix platinum wires to microneedles. The laser beam from a UV-pulsed laser (337 nm; Laser Science, Cambridge, MA) was expanded by a telescope and focused to a 4-μm spot by using a ×40 UV objective (Olympus). The glue was polymerized under UV irradiation for 10 s.

Force-Probe Calibration by Using a Platinum Filament as a Spring Reference. A 1-cm-long silver-coated platinum Wollaston wire (100-μm outer diameter, 0.6-μm inner-platinum sheath diameter; Goodfellow, Berwyn, PA) was placed on a microscope slide and held on the surface by fixing its extremities with poly(dimethyl siloxane) (PDMS) ribbons that stick to the glass. A platinum filament was obtained by removing the silver outer sheath by a 70% nitric acid treatment for 1 h and then rinsing and drying. It was then cut into a 200-μm-long filament by UV laser ablation under the microscope and fixed perpendicularly to a microneedle by optical gluing. Its rigidity was measured with the thermal-fluctuations method (27). The image of the wire was projected on a two-quadrant photodetector (United Detector Technology) with a ×1,000 magnification. Position fluctuations were recorded (with a precision of 0.2 nm) and analyzed with LABVIEW software (National Instruments, Austin, TX). The rigidity was obtained by fitting the fluctuation power fast Fourier transform spectrum with a Lorentzian (in the 10 Hz to 3 kHz frequency range). The rigidity of the filaments ranged from 0.2 to 0.8 nN/μm, with a precision ranging from 3% to 20%, depending on filament. To measure the flexible handle rigidity, the end of the platinum filament was placed against the handle at the position of the bead. While the handle was kept at a fixed position, the micropipette carrying the attached filament was translated on a 10-μm course with 0.2-μm increments by using a piezoelectric displacement (LISA; Physik Instrumente, Karlsruhe, Germany). At each step the fiber deflection was measured by tracking the bead position with the "track-object" component of METAMORPH software (Universal Imaging, Media, PA). The rigidity k' of the handle was derived from the slope p of the deflection versus displacement plot and the rigidity k of the platinum filament by using $k' = k(1 - p)/p$.

Experimental Setup. When attached on a microfiber, a 2-μm polystyrene bead (Polysciences) is coated by purified *N*-WASp (0.75 μM solution in buffer X) (20) for 10 min and then rinsed in a 1% BSA solution in buffer X. Experiments were performed in a PDMS/glass chamber, which was built as follows: a 1-mm-thick PDMS rectangle (2 × 1.5 cm) was deposited on a microscope slide and a 1 mm large L-shape channel is cut. The chamber was filled with 25 μl of standard motility medium made from pure proteins (28) at the following concentrations: 0.1 μM Arp2–Arp3/0.1 μM gelsolin/4.2 μM ADF/2.6 μM profilin/7.4 μM actin. The optical visualization was made by using a ×60 air-phase contrast objective (Olympus) mounted on an inverted microscope (IX51; Olympus), and images were taken by a cooled Cool Snap charge-coupled device (Princeton Instruments, Trenton, NJ).

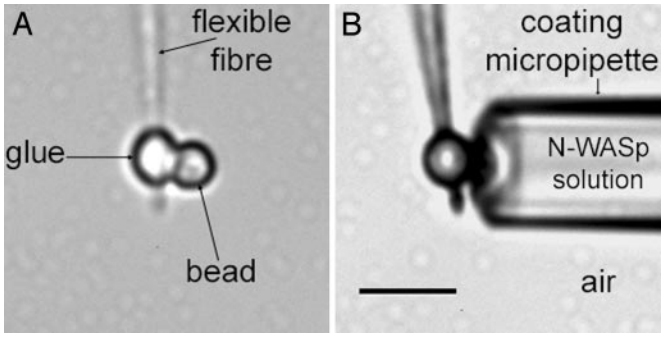

Fig. 1. The flexible handle and transmitted light images in air. (*A*) A handle made of a 2.1-μm polystyrene bead fixed to a fiber via a polymerized optical glue droplet. The handle rigidity is 4.1 nN/μm. (*B*) Coating of the handle bead. The bead is inserted in the tip of a micropipette (4.6-μm inner diameter) filled with a 0.75 μM *N*-WASp solution. The bead is in contact with the solution, whereas the rest of the handle (glue droplet and fiber) remains in air. (Scale bar, 5 μm.)

Experiment Automation. For any kind of experiment, the force is measured by tracking the bead position every ≈0.3 s on small images (≈10 × 5 μm^2) centered on the bead by using the track-object component of METAMORPH software (Universal Imaging). The zero force is determined by locating the bead position on the small image before comet handling. Every 30 steps (≈9 s), a large image (50 × 40 μm) is taken to visualize the handle and the entire comet.

For fast-pulling experiments, the micropipette is displaced by an amount proportional to the imposed velocity and the time interval between two tracks.

For force–velocity experiments, a feedback loop is used to apply a constant force on the system (equivalent to a constant deflection). For each step, the proportional feedback loop (custom program) calculates the displacement to apply to the micropipette to correct the deflection that is imposed within a 30-nm error. The maximal correction speed is 18 μm/s.

Comet-Dimensions Measurements. The diameter of the actin tail is measured as follows. The intensity (from the phase contrast image) is measured along a line perpendicular to the axis of the actin tail at a distance half-way between the handle and the micropipette. Each data point is the averaged density recorded over a 0.5-μm-wide band across this line. The diameter is defined as the distance between the minimum and the maximum of the intensity derivative over distance. The precision is 0.2 μm. The length of the actin tail equals the distance between the bead and the micropipette and is measured manually on the image with a precision of 0.1 μm.

Results

Experimental Design. Forces generated by actin polymerization are measured by using a flexible handle made of a bead attached to a glass fiber (Fig. 1*A*). A 2-μm bare polystyrene bead is fixed to any type of glass fiber (see *Materials and Methods*) by micromanipulation and gluing under the microscope as follows. A suspension of 2-μm polystyrene beads in pure water is deposited in the PDMS/slide well. A drop of glue is placed on the slide, 5 mm away from the well. The fiber tip is plunged into the glue and pulled out quickly. The glue remaining on the tip forms a droplet 1–2 μm in diameter depending on the speed at which the tip of the fiber was pulled. One bead is then grabbed off the suspension, held by suction with a micropipette of 1.5-μm inner diameter mounted perpendicularly to the fiber. The bead is driven in air and put into contact with the fiber-tip droplet. The microscope stage, on which the whole micromanipulating setup

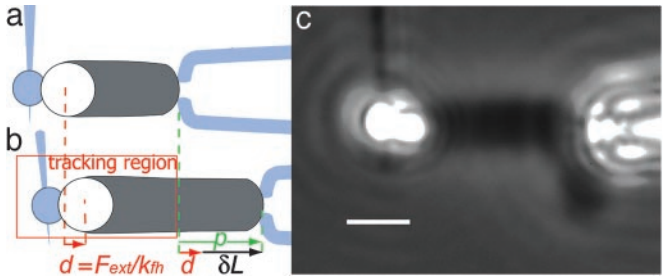

Fig. 2. Experimental scheme and image. (*a*) The actin comet (dark gray) grows from the flexible handle bead (white) and is held at its end by the comet holding micropipette. (*b*) The micropipette is moved to the right of the figure. Consequently, the bead is submitted to a force *F* proportional to the flexible handle rigidity, k_{fh}, and the deflection of the fiber *d*, measured by tracking the bead position in the tracking region. The distance, δL, is the lengthening of the comet, and it corresponds to the traveled distance of the micropipette minus the deflection. (*c*) Phase contrast image of a typical experiment. A comet (3.1-μm diameter) has grown from the bead and has been attached to the comet-holding micropipette (aperture 1.3 μm) by suction. The comet is pulled with a constant force of -0.94 nN, resulting in a slight inclination of the fiber. (Scale bar, 5 μm.)

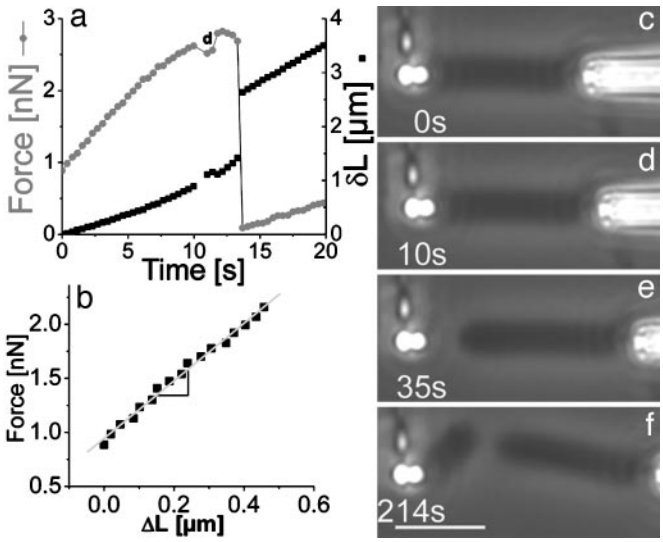

Fig. 3. Fast-pulling, detachment, and regeneration of a comet. The comet is pulled with a constant micropipette velocity of 10 μm/min. (*a*) Force (circles) and relative distance δL (squares) as a function of time. Force is obtained by multiplying the handle deflection by its rigidity (in this case, k_{fh} = 2.25n N/μm). The small force drop (δL jump) $\approx$10 s is due to the comet growth during recording of the image shown in *d* (during 1 s). The force increase after detachment might be due to some invisible actin filaments still connecting the comet to the handle. (*b*) The force as a function of the comet lengthening δL. Force versus lengthening is linear with a slope of 2.7 nN/μm, corresponding to the comet rigidity. (*c–f*) Phase-contrast images of the corresponding experiments. (*c*) Comet before fast-pulling. (*d*) Comet before pulling out. (*e*) Clean rupture of the comet from the bead surface. In *f*, a new comet has grown from the bead. The bending of the new comet can be related to the force increase explained for *a*. Time is indicated on the bottom left of the image. (Scale bar, 10 μm.)

is fixed, is moved to match the bead fiber contact zone with the UV-laser spot position. The glue is then polymerized by firing the laser for 10 s. The fiber-bound bead is then released from the micropipette by applying an overpressure. An example of an attached bead is given in Fig. 1*A*. The handle is then calibrated with a spring reference. The rigidities of the flexible handles vary from 0.8 to 4 nN/μm for pulled fibers and from 0.2 to 0.8 nN/μm for glass microfibers.

By using a micropipette as a reservoir, the bead at the end of the flexible handle is coated with the protein *N*-WASp. The micropipette (4.5-μm tip inner diameter) is filled with the solution of *N*-WASp. The handle is rinsed in pure water and set in air under the microscope. The handle bead is inserted in the micropipette tip while the rest of the handle remains in contact with air to make sure that *N*-WASp is adsorbed exclusively on the bead surface (Fig. 1*B*). After 10 min at room temperature, the bead is released from the micropipette and the whole handle is covered with BSA (1% solution) and left 5 min for incubation to saturate all available adsorption sites. The handle is driven out from the BSA solution and then placed in one branch of the L-shape cell channel that was filled previously with the motility medium. A micropipette filled with X buffer is inserted in the other branch of the channel to hold the actin comet (Fig. 2). It is mounted on the piezoelectric displacement and connected to a syringe. The sample is then covered by liquid PDMS (500 cst; 5×10^{-4} m^2/s) to prevent evaporation. As soon as the flexible handle is in the motility medium, actin polymerizes at the bead surface and an actin tail grows from the bead within a few minutes at a rate within the range of velocities measured for 2-μm free beads in the same medium (1–3 μm/min). The depolymerization is very weak, and comets can reach lengths of up to hundreds of micrometers for several hours (up to 15 h).

The comet is held with a micropipette as described for chromosomes (29). The tip is brought close to the comet distal end, and a negative pressure is applied by moving the syringe with a micropositioner, thus drawing the actin gel toward the tip. Because the aperture of the tip is at least two times smaller than the comet section, the gel stop-gaps the micropipette (see Fig. 2*c*). Note that the strength of the actin gel is sufficient to hold the local shear applied at the aperture section. The applied pressure is large enough for the comet to remain blocked on the tip while applying pulling or pushing forces up to several nanonewtons for tens of minutes.

The force is applied to the bead–comet system by moving the comet holder (Fig. 2*a*) along the comet axis with the piezoelectric displacement. Our experimental design allows for pushing or pulling on the comet. Under such an action, the flexible handle is deflected and its deflection, *d*, is proportional to the force applied on the bead. This deflection (Fig. 2*b*) is measured by tracking the bead position on small images (Fig. 2*b*; tracking region). Pushing forces up to 4.3 nN and pulling forces up to 3 nN can be applied.

Pulling the Actin Comet. By pulling on the actin tail, one can impose larger velocities than the "natural" zero load velocity for free beads. Various different experiments can be processed: the comet can be gently pulled or quickly torn away from the bead, which is the case on which we will focus now. Under fast-pulling at a constant micropipette velocity of 10 μm/min, three regimes are observed. First, the comet remains attached to the bead and sustains the force imposed by the deflected fiber (Fig. 3*d*). Under such conditions, the comet lengthens by an amount $\delta L = p - d$, as defined in Fig. 2. Then follows a nonlinear regime in which the force reaches a maximum (2.8 nN in the case presented in Fig. 3*a*). Subsequently, there is an abrupt drop of the force while δL jumps to a higher value. This event corresponds to a rupture of the bead–comet connection (Fig. 3*e*). The bead appears to be bald; the rupture of the comet occurs exclusively at the bead surface. Remarkably, after the comet has been torn off, a new comet is still able to grow from the bead. The new growing comet has identical properties (same speed, geometric characteristics, and density) as the previous comet (Fig. 3*f* and Movie 1, which is published as supporting information on the PNAS web site). The ability to rebuild a gel allows us to perform various

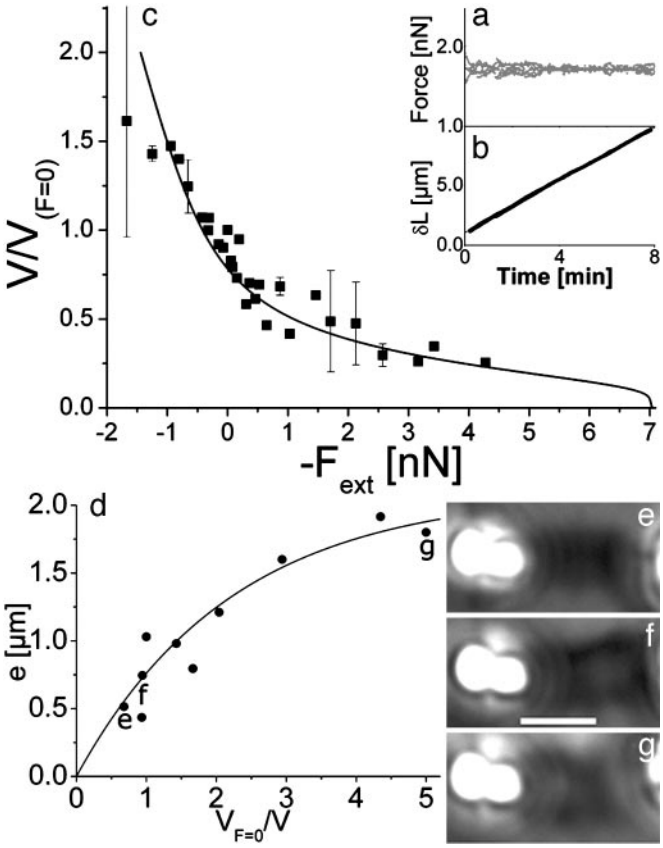

Fig. 4. Force–velocity diagram. (*a* and *b*) Typical measurement for one point of the force–velocity diagram. Force (*a*) and comet lengthening δL (*b*) as a function of time. The force is set to 1.7 nN (pushing force). The bursts are caused by small feedback-loop oscillations. The velocity is obtained from the slope of the δL versus time plot: $V = 1.1 \pm 0.15$ μm/min (the zero force–velocity for this handle is $V_{F=0} = 2.0$ μm/min). (*c*) Force–velocity relation. The velocity is normalized by the velocity at zero force measured for each flexible handle (eight different flexible handles were used). The points with an error bar are an average of two to three experiments corresponding to the same force. The relation is fitted by the equation $-F_{ext} = (E/R)e^{*3}[1 - \exp(-(x_c/x))]^3 - \xi S V_{F=0} x$, where $x = V/V_{F=0}$ and $x_c = V_p^0 R/V_{F=0}e^*$, adjusting E and ξ. (*d*) Gel-thickness dependence with speed: e is plotted as a function of the inverse of the normalized velocity $V_{F=0}/V$. Data come from two different handles. The plot is fitted by the equation $e = e^*[1 - \exp(-(x_c/x))]$, adjusting e^* and x_c. (*e–g*) Images of comets for different values of velocity corresponding to data points in *d*. (Scale bar, 5 μm.)

consecutive experiments on a single flexible handle and show that the *N*-WASp proteins are preserved in the process.

Force–Velocity Diagram: Pushing and Pulling on the Actin Tail with a Constant Force. By using this experimental design, a constant force in the −1.7 to 4.3 nN range is applied to the actin-propelled bead, and the associated velocity is measured, yielding to a force–velocity diagram. The convention for the sign of the force is that pushing forces (opposing free-bead movement) have a positive value to keep the convention that has been used in studies (20, 21, 30). This force is then the opposite of the external force, $-F_{ext}$, applied to the bead. A constant force is applied by a feedback loop. Under this condition, the velocity is well defined during this process and can be identified with the stationary velocity (smaller or larger than the zero force speed for positive and negative forces, respectively) in the 0.35–3.5 μm/min range. Fig. 4 shows an example of a 1.7 nN imposed force during 8 min (Fig. 4*a*). The comet lengthens (Fig. 4*b*) with a constant velocity of 1.1 μm/min. See Movie 2, which is published as supporting information on the PNAS web site, for a movie of a typical experiment (force −0.94 nN).

The force–velocity diagram is displayed in Fig. 4*c*. Each point corresponds to an average of one to three experiments made at constant force in a single run. For each flexible handle, the velocity $V_{F=0}$ measured at zero force is used to normalize the velocity at a given force (vertical axis of Fig. 4*c*). Note that the value of $V_{F=0}$ varies from handle to handle because of fluctuations in the coating process and different activity of protein batches. Its average value of 1.75 ± 0.6 μm/min is measured on eight flexible handles. The normalized velocities are between 0.2 and 1.7 for forces ranging from −1.7 to 4.3 nN.

For pulling forces, the force–velocity relation is essentially linear. For pushing forces, the normalized velocity decreases more gently as the force is increased. A force of 4.3 nN is not sufficient to stop the growth of the actin comet. Under such a load, the velocity is 20% of the velocity at zero load. Because of comet buckling under larger forces, the value of the stall force cannot be reached experimentally, but a lower estimate is 4.3 nN.

The gel thickness e on the side of the bead is extracted from the comet-diameter values (ϕ) measured in a subset of constant-force experiments using simply $e = (\phi - 2R)/2$, where R is the bead radius. This thickness increases when the velocity decreases, and it tends to saturate for the smallest velocity values (Fig. 4*d*). Note that the comets appear to be hollow for small velocities (large opposing forces) as can be seen in Fig. 4*g*.

Discussion

We have designed an experiment to explore the mechanics of actin-based propulsion. The flexible handle system permits us to apply both pushing and pulling forces, up to several nanonewtons, to the growing actin meshwork dynamically coupled to the propelled bead. We now discuss the measurements of the mechanical properties of the actin gel, its attachment to the bead surface, and the force–velocity relation.

Estimation of the Elastic Modulus of the Actin Tail. From fast-pulling experiments, we can estimate the elastic modulus of the actin comet. When it is pulled at a velocity larger than the free-growing velocity, the actin tail undergoes an elastic deformation. As a consequence, the force-versus-lengthening curve is linear (Fig. 3*b*) because the contribution of the comet growth is negligible compared with the elastic deformation. Its slope equals the rigidity, k_c, of the comet. The elastic modulus E of the gel is then obtained with the equation

$$E = \frac{dF}{d\Delta l_e} \times \frac{l_c}{S_c} = k_c \frac{l_c}{S_c}$$

(31), where l_c and S_c are the comet length and section, respectively, measured by image analysis. Measurement of the elastic modulus from 11 experiments yields an average value of 3,700 Pa with a lower bound of 700 and a higher bound of 6,700. This value is consistent with the one measured previously for *Listeria* in platelets–*Xenopus* extract by using optical tweezers to buckle comet fragments (32), which is 10^3 to 10^4 Pa.

Tearing the Comet Apart. Because the rupture occurs always at the bead surface, it is likely that the gel breaks at the bead–gel interface behaving as it would in an adhesive rupture event. The fact that a new actin tail resumes initiation and growth after removal of the original tail indicates that the *N*-WASp molecules remain at the surface of the bead and that the weakest points of the system are the links between the filaments and immobilized *N*-WASp. Interestingly, the process of pulling out the actin tail does not damage the activating function of the proteins immobilized at the bead surface.

The pull-out force is 3.0 ± 0.5 nN at the pulling velocity of 10

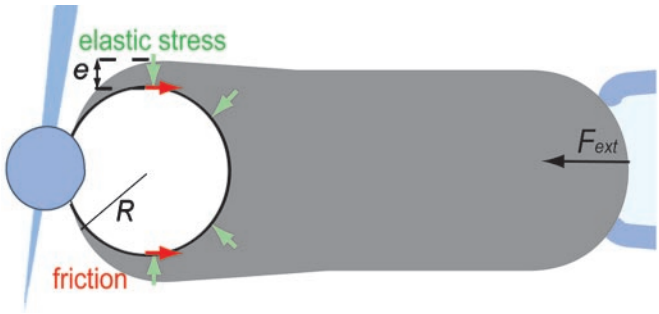

Fig. 5. Schematic representation of the elastic analysis in the case of a pushing external force F_{ext}. Green arrows indicate normal elastic stress in the gel layer of thickness *e*. Red arrows indicate friction occurring at the gel–bead interface.

μm/min. Although it is known that such a force depends on the velocity at which the object is pulled (33), we obtain here an estimate of the force necessary to detach the comet from the bead. The relevant parameter to describe the strength of the attachment is the stress applied by the actin gel on the bead. We cannot precisely measure the surface of the bead coated with *N*-WASp. However, taking the total bead surface gives a lower estimate of the stress applied on the bead surface of 0.25 nN/μm^2.

Force–Velocity Relation. The force–velocity relation characterizes the ability for a moving object to sustain its velocity while a load is applied. In the case of *L. monocytogenes*, it is an important feature because these bacteria have to cross cell membranes to disseminate: they must keep moving against the force exerted by these obstacles. Various force–velocity relations have been predicted by different theoretical models of actin-based propulsion (30, 34–36) (see ref. 37 for review). Mogilner and Oster (30) propose that within a microscopic model, the relation is essentially biphasic with a rapid decay for small forces and a smooth one for higher forces. They indicate that the decay can be less pronounced when the number of filaments is increased. Carlsson (34) finds a similar relation for the dendritic nucleation scheme but with essentially no decrease in velocity in relation with force for the autocatalytic filament branching scheme. By using a mesoscopic elastic analysis, Gerbal *et al.* (36) find a shallow force–velocity curve and predict that forces of the order of nanonewtons are necessary to slow down *Listeria* movement significantly. Two independent experiments in which external forces were applied on actin-propelled objects by adjusting the external viscosity led to differing results (20, 21). A sharp velocity drop at very low forces (10 pN) followed by a slow decrease is observed for *Listeria* in extracts, whereas beads in a pure reconstituted protein medium display a very weak decrease in velocity over a similar force range. Both studies were limited to forces of 100–200 pN. Here, we are able to apply larger forces of a few nanonewtons.

Let us now examine the experimental results in the light of the elastic analysis initially proposed by Gerbal *et al.* (36) and use a simplified formulation based on a dimensional analysis (38). In spherical topology, the addition of monomers at the internal surface of the gel generates a strain in the gel layer covering the bead. The associated tensile stress is maximum at the external surface of the gel layer and vanishes at the inner surface. It integrates into a net tension of the layer, which in the presence of curvature translates into a normal stress similar to a Laplace pressure at the gel–bead interface. This normal stress (Fig. 5) creates a propulsive polymerization-based elastic force, F_{el}, when integrated over the bead surface. The external force, F_{ext}, creates an additional stress in the gel. This stress being conservative ($\nabla\bar{\bar{\sigma}} = \bar{\bar{0}}$), its integration on the bead-gel interface equals precisely the external force. Thus, this force is entirely transmitted at the bead–gel interface. The motion of the gel with respect to the bead generates a friction F_{fric} because of the dynamical interaction between the gel and the actin polymerization activators. Let us concentrate on the simple case of a hollow comet. Indeed, we show in *Supporting Text*, which is published as supporting information on the PNAS web site, that it is a valid procedure because the contribution of the inner part of the comet (light gray in Fig. 6, which is published as supporting information on the PNAS web site) is negligible. In that case, one can directly balance the external force and the elastic force by the friction force at the bead–gel interface:

$$F_{ext} + F_{el} + F_{fric} = 0. \quad [1]$$

F_{el} reads $F_{el} \cong E(e^3/R)$ (38, ¶), where E is the elastic gel modulus, e is the gel thickness on the side of the bead, and R is the bead radius. We assume that the elastic modulus is constant and does not depend on the applied force.

The friction force may be expressed as $F_{fric} = -S\xi V$ for small-enough gel–bead relative velocity V, where S is the gel–bead contact surface and ξ is a friction coefficient per unit area (36). This term results from the finite lifetime of the activator–actin filament association (39).

The dimensional relation between the external force and the velocity becomes:

$$F_{ext} + E\frac{e^3}{R} \cong S\xi V. \quad [2]$$

One still needs to express the velocity dependence on the gel thickness. A good description of the experimental data are obtained with the empirical formula:

$$e(V) = e^*\left[1 - \exp\left(-\frac{V_p^0 R}{Ve^*}\right)\right]. \quad [3]$$

This formula interpolates between two natural limits. For small velocities close enough to stalling condition, the gel thickness is that of the steady state gel thickness e^* obtained in spherical geometry in the absence of symmetry breaking (18). For large velocities, the gel thickness is given by the polymerization rate V_p^0 multiplied by the time (R/V) spent by the gel at the surface of the bead: $e = R(V_p^0/\mathrm{V})$.

The fit of the relation between e and V according to Eq. **3** is quite satisfactory (Fig. 4*d*) and gives $e^* = 2.0 \pm 0.2$ μm and $V_p^0/V_{(F=0)} = \pm 0.3$, providing an estimate of the polymerization velocity $V_p^0 \cong 1.6 \pm 1.1$ μm/min. The subsequent fit of the experimental data points linking velocity to force involves only two parameters: the surface friction coefficient ξ and the elastic modulus E (Fig. 4*c*). For large positive forces, the friction term dominates the response. For vanishing forces, a balance between the elastic force and the friction force takes over. For significant external negative forces, the response is essentially due to the elastic force. Because the gel thickness increases when the opposing force increases, the resulting motion exhibits natural self-strengthening. We find $\xi \cong 3.10^{10}$ Pa·s/m and $E \cong 10^3$ Pa. Because Eq. **3** is a scaling relation, these numbers have a meaning only in terms of order of magnitude. It is interesting to note that the elastic modulus value agrees within a factor of 4 with our measurement extracted from fast-pulling experiments. Similarly, the friction value lies within the range estimated in ref. 36. The ratio $E/\xi = V_i$ is a velocity characteristic of the

¶Note that, in principle, we should use $F_{el} = E/Re^3(1 + e/2R)$. We checked that this does not lead to any significant change in the data analysis.

gel–surface interaction (38). We find $V_i \cong 2\ \mu$m/min, comparable with V_p^0. The similarity of the two values is not entirely fortuitous: a large mismatch would generate large stresses at the bead-inner gel interface, which would lead to hollow comets (36). In fact, close to stall force, we do see such hollowness (Fig. 4g) because of the external stress. At last, the fitting curve predicts that the stall force value is of the order of 7 nN.

Conclusion

We present a force probe experiment that allows for the control of the velocity of actin polymerization under an external force. Our data give the force–velocity diagram for both pushing and pulling forces. The force–velocity diagram is in agreement with an elastic analysis of the system. It provides numbers for the pull out force, the gel elastic modulus, the gel–bead friction coefficient, the polymerization velocity, and an estimate of the stall force. This experimental setup paves the way for investigation of actin gel properties on the efficiency of actin-based propulsion because it provides a direct measurement of the force. It might be used for testing the effect on force generation directly when drugs acting on actin assembly are at work.

We thank S. Wiesner for his help in using the purified proteins, P. Martin for his help in the calibration procedure, J. F. Joanny for fruitful discussion, A. Van Oudenaarden and one of the referees for useful comments, and J. Plastino for careful reading of the manuscript. This work was supported by an Institut Curie grant (to C.S.); a Ligue Nationale Contre le Cancer grant (to M.-F.C.) and fellowship (to Y.M.); and Human Frontier Science Program Grant RGP0072/2003 (to M.-F.C.). Y.M. was also supported by a fellowship from the Luxembourg Ministry of Research.

1. Bray, D. (2001) *Cell Movements* (Garland, New York).
2. Friedl, P. & Wolf, K. (2003) *Nat. Rev. Cancer* **3,** 362–374.
3. Merrifield, C. J., Moss, S. E., Ballestrem, C., Imhof, B. A., Giese, G., Wunderlich, I. & Almers, W. (1999) *Nat. Cell Biol.* **1,** 72–74.
4. Taunton, J., Rowning, B. A., Coughlin, M. L., Wu, M., Moon, R. T., Mitchison, T. J. & Larabell, C. A. (2000) *J. Cell Biol.* **148,** 519–530.
5. Tilney, L. G. & Portnoy, D. A. (1989) *J. Cell Biol.* **109,** 1597–1608.
6. Frischknecht, F. & Way, M. (2001) *Trends Cell Biol.* **11,** 30–38.
7. Marx, J. (2003) *Science* **302,** 214–216.
8. Pollard, T. D. & Borisy, G. G. (2003) *Cell* **112,** 453–465.
9. Mullins, R. D., Heuser, J. A. & Pollard, T. D. (1998) *Proc. Natl. Acad. Sci. USA* **95,** 6181–6186.
10. Svitkina, T. M. & Borisy, G. G. (1999) *J. Cell Biol.* **145,** 1009–1026.
11. Cameron, L. A., Svitkina, T. M., Vignjevic, D., Theriot, J. A. & Borisy, G. G. (2001) *Curr. Biol.* **11,** 130–135.
12. Loisel, T. P., Boujemaa, R., Pantaloni, D. & Carlier, M. F. (1999) *Nature* **401,** 613–616.
13. Pantaloni, D., Le Clainche, C. & Carlier, M. F. (2001) *Science* **292,** 1502–1506.
14. Borisy, G. G. & Svitkina, T. M. (2000) *Curr. Opin. Cell Biol.* **12,** 104–112.
15. Pantaloni, D., Boujemaa, R., Didry, D., Gounon, P. & Carlier, M. F. (2000) *Nat. Cell Biol.* **2,** 385–391.
16. Rogers, S. L., Wiedemann, U., Stuurman, N. & Vale, R. D. (2003) *J. Cell Biol.* **162,** 1079–1088.
17. Cameron, L. A., Footer, M. J., van Oudenaarden, A. & Theriot, J. A. (1999) *Proc. Natl. Acad. Sci. USA* **96,** 4908–4913.
18. Noireaux, V., Golsteyn, R. M., Friederich, E., Prost, J., Antony, C., Louvard, D. & Sykes, C. (2000) *Biophys. J.* **78,** 1643–1654.
19. Bernheim-Groswasser, A., Wiesner, S., Golsteyn, R. M., Carlier, M. F. & Sykes, C. (2002) *Nature* **417,** 308–311.
20. Wiesner, S., Helfer, E., Didry, D., Ducouret, G., Lafuma, F., Carlier, M. F. & Pantaloni, D. (2003) *J. Cell Biol.* **160,** 387–398.
21. McGrath, J. L., Eungdamrong, N. J., Fisher, C. I., Peng, F., Mahadevan, L., Mitchison, T. J. & Kuo, S. C. (2003) *Curr. Biol.* **13,** 329–332.
22. Upadhyaya, A., Chabot, J. R., Andreeva, A., Samadani, A. & van Oudenaarden, A. (2003) *Proc. Natl. Acad. Sci. USA* **100,** 4521–4526.
23. Giardini, P. A., Fletcher, D. A. & Theriot, J. A. (2003) *Proc. Natl. Acad. Sci. USA* **100,** 6493–6498.
24. Abraham, V. C., Krishnamurthi, V., Taylor, D. L. & Lanni, F. (1999) *Biophys. J.* **77,** 1721–1732.
25. Evans, E., Ritchie, K. & Merkel, R. (1995) *Biophys. J.* **68,** 2580–2587.
26. Cluzel, P., Lebrun, A., Heller, C., Lavery, R., Viovy, J. L., Chatenay, D. & Caron, F. (1996) *Science* **271,** 792–794.
27. Howard, J. & Hudspeth, A. J. (1987) *Proc. Natl. Acad. Sci. USA* **84,** 3064–3068.
28. Wiesner, S., Boujemaa-Paterski, R. & Carlier, M. F. (2002) in *Methods in Microbiology*, eds. Sansonetti, P. & Zychlinsky, A. (Academic, New York), Vol. 31.
29. Houchmandzadeh, B., Marko, J. F., Chatenay, D. & Libchaber, A. (1997) *J. Cell Biol.* **139,** 1–12.
30. Mogilner, A. & Oster, G. (2003) *Biophys. J.* **84,** 1591–1605.
31. Landau, L. & Lifshitz, E. M. (1967) *Theory of Elasticity* (Mir, Moscow).
32. Gerbal, F., Laurent, V., Ott, A., Carlier, M. F., Chaikin, P. & Prost, J. (2000) *Eur. Biophys. J.* **29,** 134–140.
33. Evans, E. & Ritchie, K. (1999) *Biophys. J.* **76,** 2439–2447.
34. Carlsson, A. E. (2003) *Biophys. J.* **84,** 2907–2918.
35. Carlsson, A. E. (2001) *Biophys. J.* **81,** 1907–1923.
36. Gerbal, F., Chaikin, P., Rabin, Y. & Prost, J. (2000) *Biophys. J.* **79,** 2259–2275.
37. Upadhyaya, A. & van Oudenaarden, A. (2003) *Curr. Biol.* **13,** R734–R744.
38. Prost, J. (2001) in *Physics of Bio-Molecules and Cells*, eds. Flyvbjerg, H., Julicher, F., Ormos, P. & David, F. (Springer, Les Houches, France), pp. 215–236.
39. Tawada, K. & Sekimoto, K. (1991) *J. Theor. Biol.* **150,** 193–200.